Experimental study and numerical simulation of preform or sheet exposed to infrared radiative heating

S. Monteix, Yannick Le Maoult, Fabrice Schmidt, R. Ben Yedder, R. Diraddo, D. Laroche

Experimental study and numerical simulation of preform or sheet exposed to infrared radiative heating

S. Monteix[a,*], F. Schmidt[a], Y. Le Maoult[a], R. Ben Yedder[b], R.W. Diraddo[b], D. Laroche[b]

[a]*Ecole des Mines d'Albi Carmaux, France*
[b]*Industrial Materials Institute National Research Council of Canada, Canada*

Keywords: Contour integration method; Control-volume method; Heating stage; Infrared camera; Stretch blow moulding; Thermoforming; View factor computation

1. Introduction

In both the injection stretch blow moulding and thermoforming processes, a tube- or sheet-shaped thermoplastic preform (PET, PVC, PP, etc.) must be heated before forming. In order to increase the temperature of the preform above the glass transition, infrared ovens are used [1]. Infrared heating permits a rapid heating with heat flux (proportional at the fourth power of the source temperature) occurring even on the inner surface of the preform far from the incident radiative source.

The final thickness distribution of the part is dependent on the initial temperature distribution inside the preform. It is very important to investigate parameters which determine the heating stage. They depend both on the geometrical and spectral interactions between lamps and irradiated plastic materials.

As a result of these interactions, the ratio between electric power and absorbed energy in the PET tubular preform is approximately 20%. Optimisation of the infrared oven is then necessary to allow for the control of temperature distribution and also minimisation of the energy costs. In this way, the following methodology has been applied on the heating of PET sheets:

- characterisation of infrared heaters;
- measurement of the surface temperature distribution;
- development of a three-dimensional control-volume model of the heating stage.

2. Characterisation of the heat source

The spectral properties of the infrared heaters have been already determined in the previous papers [2,3]. The infrared lamps used are sketched in Fig. 1. They are composed of a coiled tungsten filament, contained in a quartz tubular enclosure and a reflector in order to increase the heat flux efficiency to the product.

The lamps are called L300 and L400 with a nominal electric power of 300 and 400 W, respectively. The L300 is used with a cylindrical reflector made of polished aluminium. The L400 is commonly plugged into an industrial oven and fitted with a reflector made of a ceramic coating on the backside of the quartz tube as shown in Fig. 2. With a characteristic electrical power in range and a characteristic resistivity, the tungsten filament reaches steady state for the L300 at 300 W and a temperature of about 2300 K, and L400 at 400 W and a temperature of about 1700 K.

An experimental set-up (see Fig. 3) using a thermopile detector (remote sensing heat flux) was developed in order to measure the spatial directivity of the lamp.

* Corresponding author.

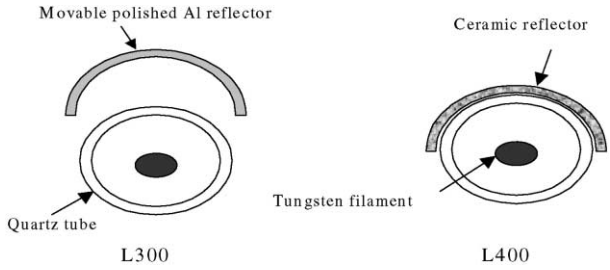

Fig. 1. Infrared heaters.

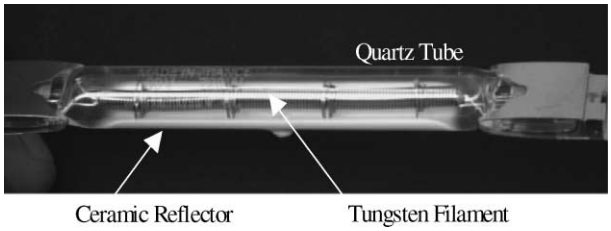

Fig. 2. Industrial heater (L400).

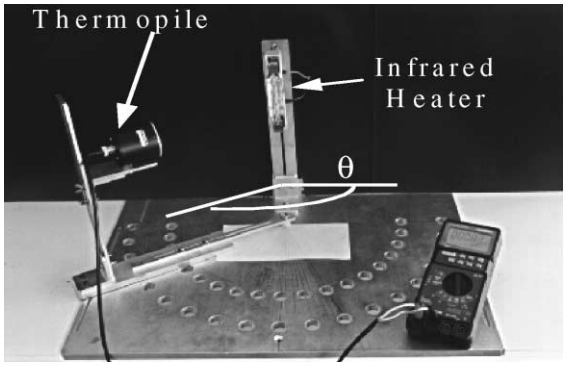

Fig. 3. Experimental set-up for infrared heaters characterisation.

The flux sensor moves a half circle around the filament in order to measure the spatial directivity of each heater. Then, it intercepts the radiation in each direction described by the angle θ. The thermopile presents a bandwidth defined between 8 and 14 μm. In this spectral range, the quartz tube presents a full absorption of the filament radiation [2]. We assume that the heaters directivity is the same as that of the quartz tube because of their concentric geometry (the cylindrical filament in the quartz tube).

The normalised intensity is plotted versus the angle θ as shown in Fig. 4. For all the measurements, the solid angle of the thermopile is centred in the middle of the lamp filament. In comparison with a Lambertian source (diffuse radiation), the lamps L400 and the L300 used without reflector are similar to an isotropic source (except some border's effects). As expected, we observe that the lamp L300 fitted with a specular reflector exhibits a strong directionality in front of the reflector.

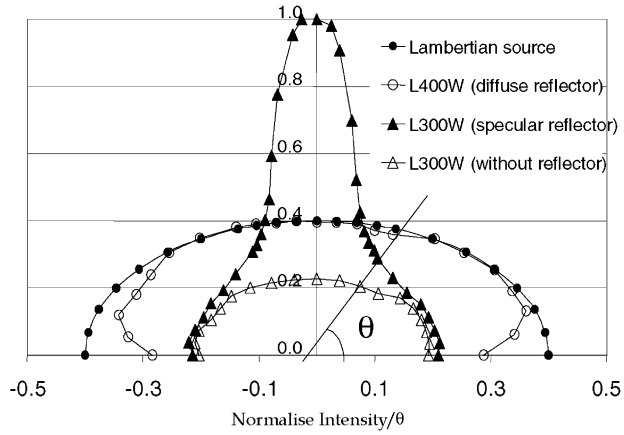

Fig. 4. Infrared heater's directivity.

3. Temperature distribution measurement

3.1. Experimental procedure

Fig. 5 shows the experimental set-up which has been developed in order to measure the surface temperature evolution when a PET sheet is heated using the infrared lamp.

An 880 LW AGEMA infrared camera (8–12 μm bandwidth) is used to evaluate in a remote sensing, the spatial and transient temperature distributions. The surface dimension of the sheet is 20 cm × 20 cm and the thickness is 1.5 mm. The distance between heaters and sheets is 5 cm. The frequency of analysis is 25 frames/s and the device is connected to a 12 bit data acquisition board drive with a real time software (Addelie®).

The camera's objective is oriented normally to the sheet's surface. However, due to the spectral absorbance of the PET [4], care is required for the surface temperature measurement [5]. To do this, the spectral absorbance of the PET must be characterised prior to determining the bandwidth where the material is assumed to be opaque (see Fig. 6). In this case, only the radiation emitted from the material surface is intercepted by the camera's sensor, although all the other radiation from the bulk or the sheet environment are absorbed before reaching the viewed surface [6].

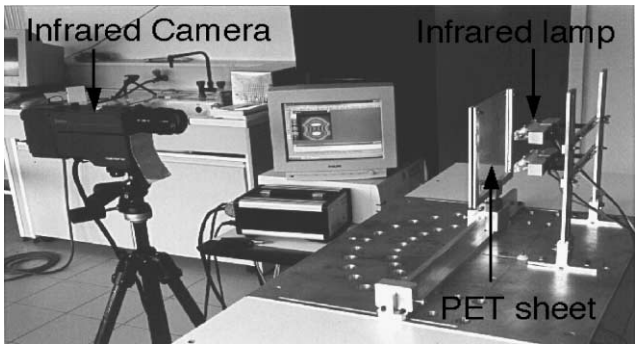

Fig. 5. Experimental heating set-up.

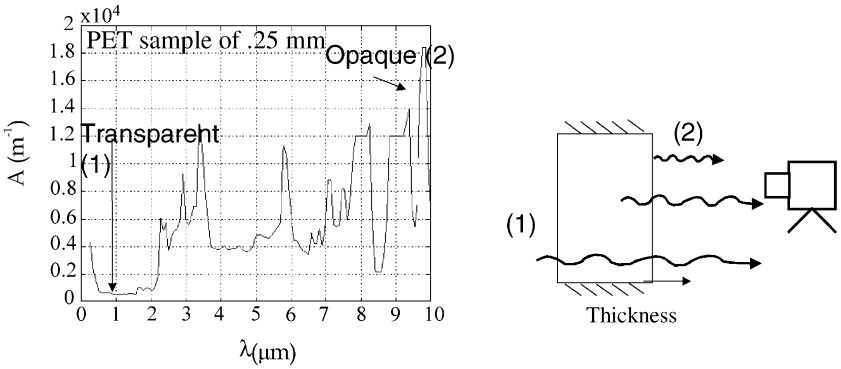

Fig. 6. The PET spectral absorbance.

Previous work deals with PET transmittivity [7], in the spectral range of the heaters intensity, defined by Wien's law for a temperature of 2300 K. In the bandwidth of the AGEMA camera (8–12 μm), there is no available data. Then in order to observe the PET behaviour, we have assessed reflectivity and transmittivity coefficients using the infrared camera and a laboratory blackbody.

4. Results

4.1. Temperatures

Measurements have been processed for 0.7 and 1.5 mm PET sheet thicknesses. Tables 1 and 2 show a very low average transmittivity on this spectral band. The average emissivity is then calculated from the reflectivity measurement.

Taking into account these characteristics, temperatures are measured during heating and cooling stages from the back and front surfaces of the sheet. It takes 3 s to bring the front face in front of the camera during which a cooling stage due to natural convection occurs.

During this transfer, a relative difference less than 0.7% appears in temperature measurements similar to a cooling with a transfer coefficient, $h = 10\,\mathrm{W\,m^{-2}\,K^{-1}}$.

Table 1
PETs transmittance (8, 12 μm; blackbody temperature = 150°C)

Thickness (mm)	τ_{sheet}
0.7	5×10^{-3}
1.5	2×10^{-3}

Table 2
Normal PET reflectance (8, 12 μm)

Blackbody temperature (°C)	ρ_{n}
70	0.06
110	0.07
150	0.07

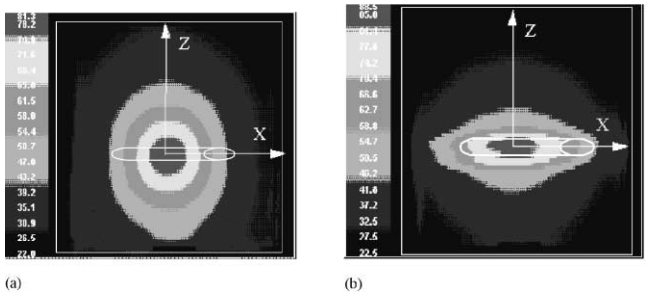

Fig. 7. (a) Diffuse reflector for thermogram for L400. (b) Specular reflector for thermogram for L300.

In Fig. 7, two infrared thermograms are presented for a heating time of 35 s. Fig. 7a shows the surface temperature distribution measured on the back face of the sheet for the heat source L400. The surface temperature distribution is relatively isotropic due to the presence of the diffuse reflector. These results confirm that the Lambertian source assumption (diffuse radiation) are valid for the lamp L400. As expected, the surface temperature distribution for the lamp L300 (specular reflector) is strongly anisotropic (see Fig. 7b).

4.2. Thermograms

In this part, thermograms for 1.5 mm PET sheet's thicknesses are examined. Thermograms recorded from the front and back faces with the same experimental heating conditions provide (Fig. 8) the measurement of the temperature gradient reached across the thickness after a heating time of about 35 s. This gradient is related to the location of the measured point on the sheet surface in association with the temperature level at this point. The highest gradient (about 8 °C) is reached at the sheet centre (the same as the heater's centre) corresponding to the highest temperature level of about 85 °C.

The temperature versus time is presented in Fig. 9 for different z-values (see Fig. 7) on the sheet. The dotted vertical line indicates the end of the heating. These measurements during the heating and cooling stages reveal a delay between the heater switch off and the record of the

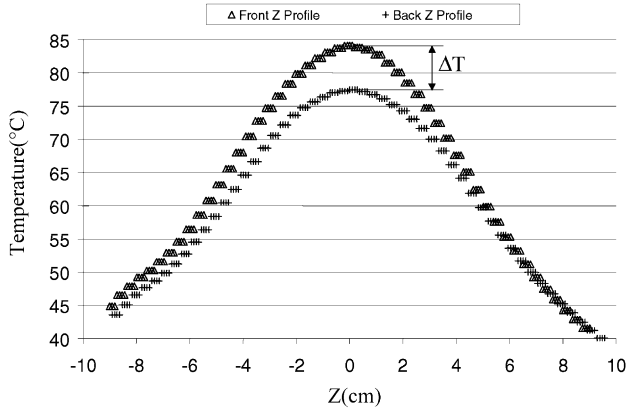

Fig. 8. Measurement of the temperature gradient after heating stops.

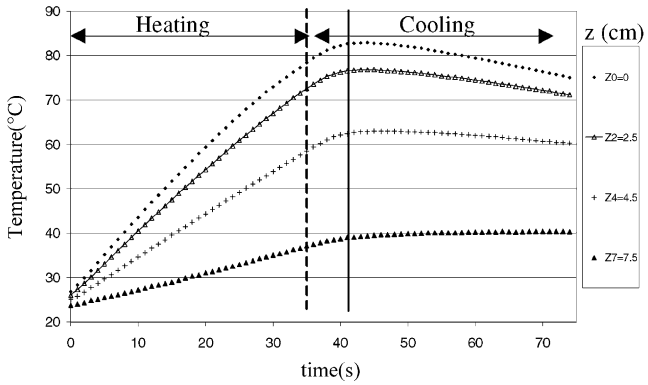

Fig. 9. Transient evolution of the temperature.

maximum temperature level from the back face. This delay (about 8 s) is less important than the time of the diffusion phenomenon in the semi-infinite sheet submitted to a surface temperature T_s. In this case, the time t_{diff} required to reach half of the initial temperature difference (between T_s and the temperature at a depth e) is equal to $t_{diff} = e^2/0.92\alpha$ [8].

The PET diffusivity $\alpha = 1.4 \times 10^7\,m^2\,s^{-1}$ which corresponds to t_{diff} equal to 17 s over the sheet thickness of 1.5 mm. This discrepancy compared to 8 s reveals the relative influence of the natural convection which tends to accelerate the equilibrium of temperature levels across the sheet thickness. In contrast, the spatial temperature distribution after the same equilibrating time presents a larger difference on the z-axis. This means that the one-dimensional radiative transfer throughout the thickness is more influent than the conductive transfer in any direction of the space.

5. Control-volume formulation

A three-dimensional control-volume model has been developed for computing the radiative heat transfer during the infrared heating stage. The sheet-shaped domain sketched in Fig. 10 is discretised into cubic elements called control volumes [9]. The temperature balance (Eq. (1)) including radiative transfer (thermal power absorbed by the polymeric sheet from the infrared heaters) is integrated over each control volume and over the time from t to $t + \Delta t$. $V = \Delta x \Delta y \Delta z$ is the control volume, $\vec{q_c}$ the Fourier's flux ($\vec{q_c} = -k\nabla T$), $\vec{q_r}$ the internal radiative heat flux. The unknown temperatures are computed at the cell centres. The heat conductivity k, the specific mass ρ as well as the heat capacity C_p are assumed to be constant in agreement with previous work [10]:

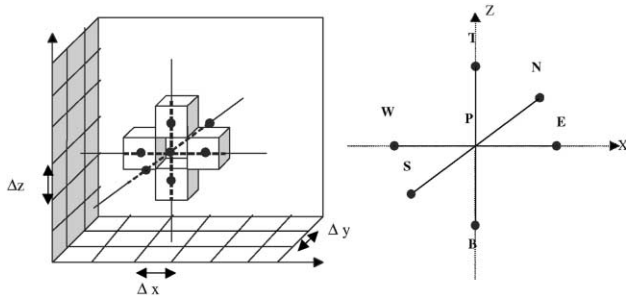

Fig. 10. The sheet shape mesh.

$$\int_{\Delta t}\int_{V} \rho C_p \frac{\partial T}{\partial t}\,dV\,dt = -\int_{\Delta t}\int_{V} \vec{\nabla}(\vec{q_c} + \vec{q_r})\,dV\,dt \qquad (1)$$

5.1. Amount of incident radiation

Previous works [11,12] dealt PET sheet's heating with a radiant heat flux uniform all around the radiated face or assumed an arbitrary intensity without consideration about heaters dimension. Here, the specific lamp geometry is considered, taking into account from a view factor computation [13]. We assume a constant filament temperature and an uniform source temperature. Thus, the amount of incident radiation reaching each front elements of the irradiated sheet is performed with the contour integration method (Eq. (2)) using Stoke's theorem [13]:

$$F_{H\to r_s} = \frac{1}{2\pi S_H} \oiint_{\Gamma_H \Gamma_{r_s}} \ln r\,d\vec{r}_H\,d\vec{r}_{r_s} \qquad (2)$$

where the subscripts H refers to the heater and r_s to the sheet front element under consideration; S_H the heater surface, r the distance between two elemental linear elements issued from the discretisation of the entire heater border Γ_H and Γ_{r_s} for each surface of control element's border reaching the irradiated sheet's face. This contour integration method was chosen between different numerical view factor method (Monte-Carlo or geometric method). This method allows a good accuracy at a very low computational time and a simple way of use. An efficient numerical method based on Gaussian quadrature has been applied in order to perform the result of this method.

In order to take into account the participation of the diffuse reflector in the amount of the incident radiation, a coefficient of efficiency k_{rf} is introduced. k_{rf} is calculated

assuming a strip surface for both the heater and its reflector and considering all the flux emitted from this equivalent surface equal to the flux emitted from the entire filament surface [14], i.e. $S_{\mathrm{fil}} = \pi d L_{\mathrm{fil}}$ where d represents the coiled tungsten diameter equal to 4 mm and L_{fil} the length about 64 mm. Using these assumptions, we have $k_{\mathrm{rf}} = \pi$.

Thus, the amount of incident radiation $\phi(r_{\mathrm{s}})$ (Eq. (3)) on each surface element is

$$\phi(r_{\mathrm{s}}) = \phi(x, y = 0, z) = k_{\mathrm{rf}} F_{H-r_{\mathrm{s}}} \frac{S_H}{S_{r_{\mathrm{s}}}} \int_{\Delta\lambda} \varepsilon_\lambda(T_{\mathrm{fil}}) \pi L_\lambda^0(T_{\mathrm{fil}})\, \mathrm{d}\lambda \tag{3}$$

where $\varepsilon(\lambda)$ is the spectral tungsten emissivity, T_{fil} the filament temperature, L_λ^0 the blackbody intensity and λ a given wavelength between 0.2 and 10 μm.

5.2. Internal radiative heat flux

In the first approximation, internal radiative transfer is assumed to be one-dimensional across the sheet thickness. The PET bulk temperature (≈400 K) is very low in comparison to the source temperature ($T_{\mathrm{s}} = 1700$ K). So, the assumption of "cold material" is convenient. This leads to express the transmitted flux q_{r} (Eq. (4)) across the thickness (y-axis) of the sheet, for an homogenous amorphous PET, using the Beer–Lambert's law in the y-direction

$$q_{\mathrm{r}} = \phi_{\lambda}(x, y, z) = \phi_{\lambda}(x, y = 0, z)\, \mathrm{e}^{-A_\lambda y} \tag{4}$$

where $A(\lambda)$ is the spectral absorption coefficient of the material which is given in the below equation

$$A(\lambda) = -\frac{\ln \tau(\lambda)}{L} \tag{5}$$

where L is the thickness of the PET film used to obtain an intrinsic transmission coefficient $\tau(\lambda)$ and, consequently, an accurate $A(\lambda)$ dependence with wavelength.

The internal heat source S_{p} on the principal p control volume is given in the following equation:

$$S_{\mathrm{p}} = -\int_{\Delta t}\int_{V} \vec{\nabla} \cdot \phi(y) \mathrm{d}V\, \mathrm{d}t = -\int_{\Delta t}\int_{S} q_{\mathrm{r}}\, \mathrm{d}S\, \mathrm{d}t \tag{6}$$

where S are the surfaces of the control volume. We assume the incident flux direction is the same as that of the normal vector of S surfaces (see Fig. 11).

Finally, the S_{p} formulation is expressed by

$$S_{\mathrm{p}} = \phi(x, y = 0, z)[\tau_\lambda^{y_{\mathrm{s}}/L} - \tau_\lambda^{y_{\mathrm{n}}/L}] \tag{7}$$

For the next step, the integration of Eq. (1) over all the control volumes leads to a linear equations system, which is solved iteratively using the line-by-line Gauss Seidel method in the y-direction of range to obtain a three-dimensional system resolved by a tridiagonalisation method using the Thomas algorithm.

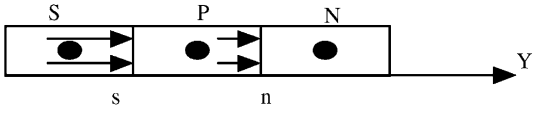

Fig. 11. Radiative internal transfer.

5.3. Validation of the numerical model

The numerical model is validated for the analytical case of a semi-infinite partially transparent solid [15], subjected to a uniform incident heat flux (q_0''). Its value is evaluated using Eq. (3) considering the entire spectrum and all the irradiated sheet surface (Eq. (8))

$$q_0'' = k_{\mathrm{rf}} \frac{S_H}{S_R} F_{H-R}(\varepsilon_{\mathrm{moy}} \sigma T_{\mathrm{fil}}^4) \tag{8}$$

In these specific conditions, the temperature $T(y, t)$ across the thickness (y-axis) versus time t is computed using Laplace's transforms in order to solve the one-dimensional energy equation with the term source per unit volume, $q_0''' \ (= q_0'' A\, \mathrm{e}^{-Ay})$ and considering adiabatic borders. The constant A corresponds to an average absorption coefficient (Eq. (9)), evaluated from Eq. (5) with an average PET's transmittivity [16]:

$$\overline{\tau} = \frac{\int_{\Delta\lambda} \tau_\lambda M_\lambda^0(T_{\mathrm{fil}})\, \mathrm{d}\lambda}{\int_{\Delta\lambda} M_\lambda^0(T_{\mathrm{fil}})\, \mathrm{d}\lambda} \tag{9}$$

The solution is given in the below equation

$$\begin{aligned} T(y,t) = T_{\mathrm{ini}} &- \frac{q_0'''}{kA}\, \mathrm{e}^{-Ay} + q_0''' \sqrt{\alpha t}\, \mathrm{i}\,\mathrm{erfc}\left(\frac{y}{2\sqrt{\alpha t}}\right) \\ &+ \frac{q_0'''}{2kA}\, \mathrm{e}^{A^2\alpha t + Ay} \mathrm{erfc}\left(A\sqrt{\alpha t} + \frac{y}{2\sqrt{\alpha t}}\right) \\ &+ \frac{q_0'''}{2kA}\, \mathrm{e}^{A^2\alpha t - Ay} \mathrm{erfc}\left(A\sqrt{\alpha t} - \frac{y}{2\sqrt{\alpha t}}\right) \end{aligned} \tag{10}$$

where T_{ini} is the initial temperature.

Analytical and numerical solutions are compared for a 100 mm × 100 mm sheet of 200 mm thickness. Its front surface is subjected to an incident radiation (9) with a filament temperature of about 1700 K, corresponding to an average tungsten emissivity of about 0.26 and an absorption coefficient of 2660 m^{-1} for a wavelength delimited between 0.2 and 10 μm. The view factor in this case between the strip heater and sheet is evaluated as 0.53.

In Fig. 12, comparisons for the temperature versus thickness are shown. The agreement is good with an error of less than 2%.

5.4. PET sheet's heating simulation

After the validation of the model, heating of thin sheets is now performed. The predicted temperature using numerical simulations are compared to experimental temperature measurements in the case of a PET sheet of 1.5 mm thickness. The heating time is 35 s corresponding to typical heating times for industrial processes.

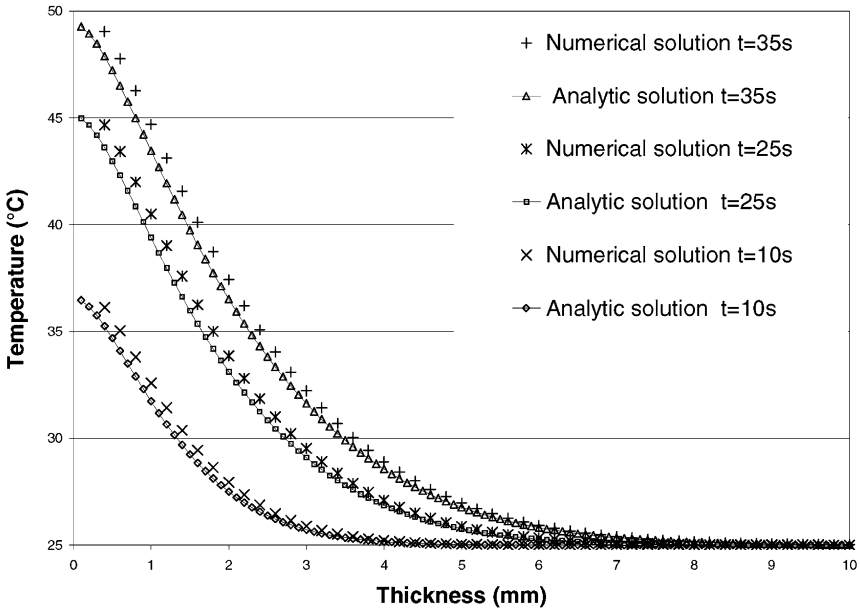

Fig. 12. Comparison between numerical and analytical temperatures versus thickness.

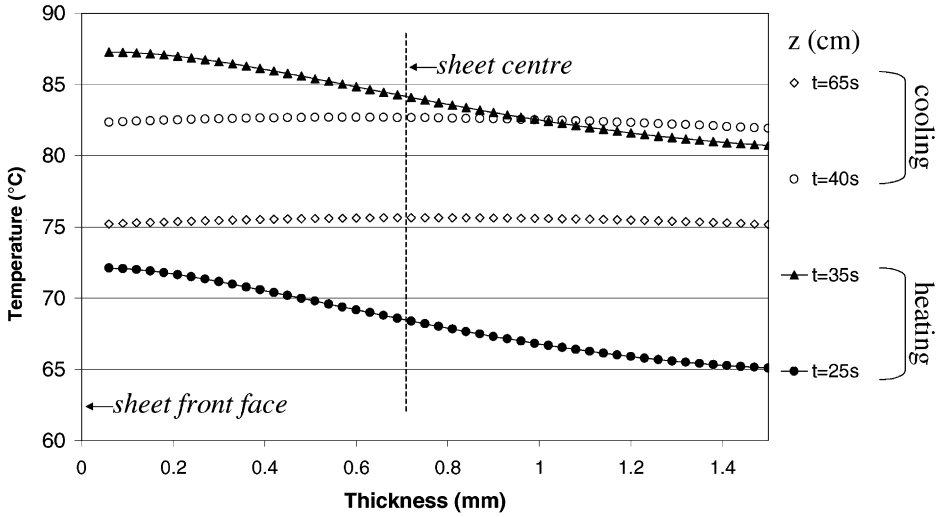

Fig. 13. Numerical temperature distribution through the thickness.

Boundary conditions are given below:

$$-k\left(\frac{\partial T}{\partial y}\right)_{y=0} = -k\left(\frac{\partial T}{\partial y}\right)_{y=e} = h(T_S - T_\infty),$$

$$\left(\frac{\partial T}{\partial x}\right)_{x=0,l} = \left(\frac{\partial T}{\partial z}\right)_{z=0,H} = 0 \qquad (11)$$

An uniform convection coefficient is applied to the back and front faces (estimated to be 10 W m^{-2} K^{-1}) [17].

The numerical modelling leads to the following temperature distribution through the sheet thickness, in particular, at the sheet centre (see Fig. 13).

During the heating time, a constant temperature gradient across the thickness equal to 7 °C appears. Then, as soon as the heating is switched off, the temperature difference between the front and back faces rapidly decreases. Five seconds are

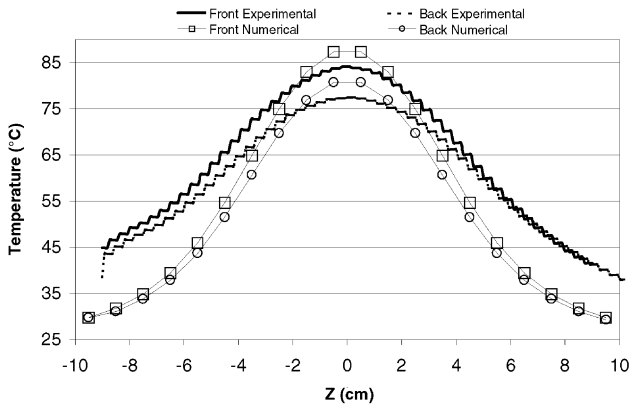

Fig. 14. Gradient temperature in the z-direction.

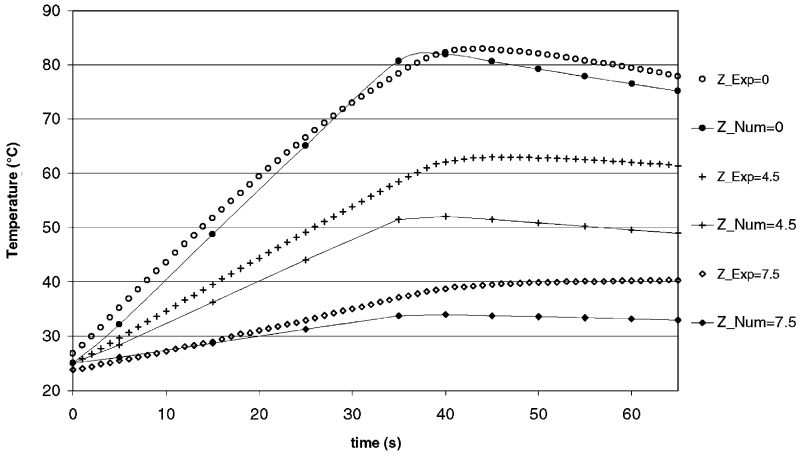

Fig. 15. Transient temperature from the back face.

sufficient to observe the establishment of an equilibrium temperature level all across the thickness. It provides a confirmation of the temperature increase, recorded experimentally from the back face as the natural cooling starts. The comparison between experimental and numerical results for the temperature profile versus z-axis is plotted in Fig. 14.

Points localised near the sheet centre and front of the heater (in a circle of 2 cm diameter), the difference between the two temperature results is less than 2%. For the other part of the sheet, the discrepancy is more important. This observation is valid for both front and back faces of the sheet. This difference is first due to the incident flux distribution on the irradiated face, more than the assumption, permitting the flux absorption only normal to the incident surface. Several reasons could explain this inaccurate incident front conditions. In particular, the numerical geometry of the strip surface assumed to be equivalent to the radiative cylindrical heater surface. Previous workers [18] have shown that the quartz tube effect is not negligible denoting a refraction of the radiative beam from the tungsten filament centred in the quartz tube. This will lead to an increase of the dispersion angle of the radiant heat flux.

In Fig. 15, the temperature profile versus time in the z-direction is plotted. We observe good agreement between experimental and numerical results near the centre of the sheet. Comparisons during the cooling stage exhibits a faster temperature decrease, in particular, at the sheet top extremity. We suppose this discrepancy is due to the one-dimensional description of internal radiative heat transfer. One-dimensional modelling leads to minimised radiative source. It is more significant when the heat flux arrived on the sheet surface with a consequent angle higher near the vertical sheet extremities.

6. Conclusion

Preliminary investigations of the infrared heater properties (spatial and spectral) fitted with diffuse reflectors allow to consider them as an isotropic radiative source. The interaction between these lamps and PET sheet has been observed using an infrared camera. The temperature distribution from the back to the front face of the sheet has allowed an estimation of temperature gradient when the heating is switched off. The heating stage of the PET sheet, submitted to an industrial infrared heater, is taking account with the one-dimensional Beer–Lambert's law computed with a control volume model. Experimental and numerical results lead to conclude that the temperature distribution through the sheet thickness (1.5 mm) attain rapidly an equilibrate temperature during the cooling stage. However, due to the poor conductivity of the PET, the non-uniform temperature distribution over the irradiated faces of the sheet still appear after the cooling stage.

Considering an efficiency reflector coefficient, the comparison between experimental and numerical results presents discrepancies higher from the centre of the sheet to the extremities due to the one-dimensional radiative heat transfer model.

Further developments will permit to take better into account the real interaction between PET preform and infrared heaters and the oven's environment:

- defining the reflector efficiency;
- observing transfer convection;
- applying this methodology to the tubular PET preform heating.

Acknowledgements

This work is supported by Perrier-Vittel Company. Special thanks goes to G. Denis, A. Contal and J.-P. Arcens.

References

[1] C. Lindenlaub, Thermoformage, Techniques de l'Ingénieur, A3660, 1982 (in French).

[2] Y. Le Maoult, F. Schmidt, M. El Hafi, Measurement and calculation of preform infrared heating, in: Proceedings of the Fourth

International Workshop on Advanced Infrared Technology and Applications, Firenze, September 1997.
[3] S. Monteix, R. Diraddo, F. Schmidt, Profiles infrared radiative heating in blow molding and thermoforming, in: PPS'98—North American Meeting, Toronto, August 17–19, 1998.
[4] K. Hartwig, Simulation of the stretch-blow molding process and characterization of the relevant material behavior, Dissertation, RWTH, Aachen, 1996.
[5] M. Lallemand, A. Souffiani, Mesure de température dans les milieux semi-transparents, Rev. Gen. Therm. (HS95) 34 (1995) 69–85 (in French).
[6] N. Haji, J.E. Spruiell, Radiation pyrometry on semitransparent sheets. I: gray media, Polym. Eng. Sci. 34 (2) (1994) 116–121.
[7] M.D. Shelby, Effects of infrared lamp temperature and other variables on the reheat rate of PET, in: Proceedings of the Conference, Antec'91, 1991, pp. 1420–1424.
[8] J.F. Agassant, P. Avenas, J.Ph. Sergent, La mise en forme des matières plastiques, Technique et Documentation, Lavoisier, 1986 (in French).
[9] S.V. Patankar (Ed.), Numerical Heat Transfer and Fluid Flow, McGraw-Hill, New York, 1980.
[10] K. Esser, Infrared radiation in the processing of plastics: precise adjustment—the key to productivity, Adv. Polym. Technol. 7 (2) (1987) 89–128.
[11] P. Lebaudy, Etude et simulation de la répartition des températures dans un cylindre creux de PET soumis a un rayonnement infra-rouge, Université de Rouen, 1989 (in French).
[12] A. Denis, Etude expérimentale et modélisation du chauffage par rayonnement infrarouge de polymères semi-cristallins: influences des centres diffusants, Université de Rouen, 1995 (in French).
[13] R. Rammohan, Efficient evaluation of diffuse view factors for radiation, Int. J. Heat Mass Transf. 39 (6) (1996) 1281–1286.
[14] S. Harmand, Contribution a la modélisation des échanges radiatifs entre un champ d'émetteurs infrarouges et un corps en déplacement, Université de Valenciennes et du Hainaut Cambresis, 1990 (in French).
[15] A. De Wriendt, La transmission de la Chaleur, Vol. 1, Tome 1, 2nd Edition, Morin (in French).
[16] R. Siegel, J.R. Howel, Thermal Radiation Heat Transfer, 3rd Edition, Hemisphere/Taylor & Francis, Washington, 1992.
[17] J.F. Sacadura, Initiation aux Transferts Thermiques, Lavoisier, 1973 (in French).
[18] T.L. Turner, Numerical and experimental analyses of the radiant heat flux produced by quartz heating systems, NASA Technical Paper No. 3387, Langley Research Center, Virginia, 1994.